Continuous electroconversion of CO_2 into formate using 2 nm tin oxide nanoparticles

Ivan Merino-Garcia[a,b,c], Lionel Tinat[d], Jonathan Albo[b], Manuel Alvarez-Guerra[b], Angel Irabien[b], Olivier Durupthy[d], Vincent Vivier[c], Carlos M. Sánchez-Sánchez[c,*]

[a] *Universidade Nova de Lisboa, FCT, Chemistry Department, Associated Laboratory for Green Chemistry-Clean Technologies and Processes (LAQV), Caparica 2829-516, Portugal*

[b] *University of Cantabria, Department of Chemical and Biomolecular Engineering, Avenida de los Castros s/n, 39005 Santander, Cantabria, Spain*

[c] *Sorbonne Université, CNRS, Laboratoire Interfaces et Systèmes Electroquimiques, LISE, 4 place Jussieu, F-75005 Paris, France*

[d] *Sorbonne Université, CNRS, Collège de France, Laboratoire de Chimie de la Matière Condensée de Paris, 4 place Jussieu, F-75005 Paris, France*

* Corresponding author; e-mail: carlos.sanchez@upmc.fr

Abstract

SnO_2 nanoparticles (NPs) are considered a suitable electrocatalyst for the production of formate from CO_2 reduction reaction (CO_2RR). We synthesize, characterize and evaluate high surface area SnO_2 NPs (2.4 nm and 299 m^2 g^{-1} in diameter size and surface area, respectively), as electrocatalyst for the continuous production of formate at high current density within a flow electrolyzer.

The stability of SnO_2 NPs under CO_2 reduction conditions was demonstrated in this work by cyclic voltammetry. SnO_2-based gas diffusion electrodes (SnO_2-GDEs) were manufactured to perform continuous CO_2RR. A maximum formate concentration of 27 g L^{-1} was achieved with a Faradaic efficiency (FE) of 44.9% at 300 mA cm^{-2}. Nevertheless, ohmic drop contribution on the SnO_2-GDEs due to the semiconducting properties of SnO_2, was not negligible. Moreover, the low total FE (< 60%) of products pointed out a leakage of formate by crossover migration through the membrane from the catholyte towards the anolyte.

Keywords: CO_2 electroreduction, formate, SnO_2 nanoparticles, Continuous reactor, Gas diffusion electrodes.

1. Introduction

The concentration of CO_2 in the atmosphere is reaching unprecedented values (413 ppm in December 2020) [1] due to the increasing depletion of fossil fuels as world energy demand continues to increase. Thus, the conversion of captured CO_2 into useful chemicals is considered one of the most efficient technologies to tackle the challenge [2–4]. Although several CO_2

activation and conversion techniques are nowadays available such as chemical, photochemical and photoelectrochemical methods [5–7], the catalytic process for the transformation of CO_2 into value-added products throughout electrochemical reactions is appealing due to the environmental and potential economic benefits. In particular, the possibility of closing the carbon cycle, as well as its strategic advantage in storing electrical energy in the form of chemical bonds, makes this technology one of the most sustainable methods currently available, in which the electrons can be derived from renewable energy sources such as wind or solar power [8]. For this reason, different approaches from both homogeneous [9–11] and heterogeneous catalysis [12,13] have been applied to the electrochemical CO_2 reduction reaction (CO_2RR).

Different commercially useful chemicals can be produced from the electrochemical conversion of CO_2 at room temperature as a function of the number of proton-coupled electron transfers required in each electrochemical reaction [14–17]. In addition to this, the selectivity of the reaction strongly depends on the catalytic material, as well as process conditions, such as the applied voltage, among others [18,19]. The main products obtained from CO_2 electroreduction can be classified in the following four categories: *i*) carbon monoxide (CO) [20,21]; *ii*) formic acid/formate ($HCOOH/HCOO^-$) depending on the pH [22,23]; *iii*) alcohols such as methanol (CH_3OH) [24] and ethanol (C_2H_5OH) [25]; and *iv*) hydrocarbons including methane (CH_4) [26] and ethylene (C_2H_4) [27]. It is vital to stress the importance of controlling the hydrogen evolution reaction (HER) [28], since the production of hydrogen from water electrolysis competes with CO_2 electroconversion, reducing, therefore, the selectivity of the electrochemical process towards the desired useful reduction product.

In this work, we study the continuous production of formate from CO_2 single-pass electrochemical conversion, in which two electrons are exchanged, at high current density within a flow electrolyzer, which allows direct feed of gaseous CO_2 to the electrochemical interface by means of a gas diffusion cathode and avoids mass limitations associated with CO_2 solubility in solution. Formate is widely used industrially in different pharmaceutical or leather industries, among others [22]. Moreover, formate can be supplied as fuel (starting from 0.5 M in solution) for direct formic acid fuel cells (DFAFCs) to produce electricity [29] and is considered one of the highest value-added CO_2 electroreduction products in terms of market price since this product reaches a value of around $1000 - $1700 per ton of product [30]. The main targets pointed out in the literature for the CO_2RR-into-formate process to become industrially feasible are [31]: *i*) reaching a formate production higher than 45 g L^{-1} (1 M); *ii*) using current densities higher than 100 mA cm^{-2}; *iii*) keeping Faradaic efficiency (FE) higher than 50% and energy consumption lower than 500 kWh $kmol^{-1}$ product; and *iv*) using continuous-flow operation mode at mild-ambient temperature and pressure conditions. Moreover, the long-term stability and durability of the working electrodes have been recently reported to be crucial for this technology to be implemented in the short term [32] and further comprehensive durability tests are still needed in the literature.

Among the different available electrocatalysts mainly producing formate from CO_2RR, metallic tin (Sn) appears to be one of the best alternatives in terms of cost and selectivity, highlighting also

its low toxicity, even though other metals such as lead (Pb) and bismuth (Bi) have also been proposed as efficient electrocatalysts for formate production [23,33–37]. Nevertheless, not only the synthesis of small size capping agent free Sn nanoparticles (NPs) is tricky, but also the structural stability of Sn NPs during CO_2 electroreduction is low, owing to Ostwald ripening dissolution and re-deposition. Furthermore, the behavior of Sn NPs under industrial (high) current density conditions represents a challenge that still needs to be solved [38]. As a consequence, either the use of oxide films on Sn electrodes or purely tin oxide (SnO_2) NPs has been recently considered in literature as suitable electrocatalytic material for the production of formate from CO_2RR [39–47], since SnO_2 presents much higher structural stability under electrochemical conditions. In particular, a lot of attention has been focused on identifying the role of the different species present on the surface of the electrode (Sn/SnO/SnO_2) during CO_2RR. This surface composition-reactivity relationship has been studied in detail by Raman spectroscopy [48] and scanning electrochemical microscopy (SECM) [49], which have demonstrated that oxide films (SnO_x) on the surface of Sn electrodes play a key role by enhancing formate production and selectivity during CO_2RR.

Therefore, the present study aims at evaluating the application of crystalline and high specific surface area SnO_2 NPs (2.4 nm in average diameter size), synthesized by a template free and facile hydrothermal microwave-assisted method, as an alternative electrocatalyst for the continuous CO_2RR into formate at high current densities. As far as the authors know, there is not one single report evaluating the activity and selectivity performance of SnO_2 NPs in a flow electrolyzer, since most of the work published so far has used SnO_2 catalyzed gas diffusion electrodes (GDEs) in a two compartments H-type cell, where poor current densities between 5 and 12.5 mA cm^{-2} were reported [42,43,45,46,50]. Only highly porous SnO_2 nanosheets supported on carbon cloth reached 70 mA cm^{-2} as current density in H-type cell [51]. Thus, the following objectives are addressed herein: *i*) synthesis and comprehensive physicochemical characterization of high surface area SnO_2 NPs; *ii*) electrochemical characterization of SnO_2 NPs deposited onto a glassy carbon electrode by cyclic voltammetry; *iii*) manufacturing of GDEs as cathodes containing SnO_2 NPs as catalyst; and *iv*) analysis of the synthesized SnO_2–GDE for the continuous CO_2RR into formate in aqueous solution, using a single-pass flow reactor configuration [52–54] to evaluate their performance operating at high current densities.

2. Experimental

2.1. Synthesis of SnO_2 nanoparticles

The synthesis of the SnO_2 NPs has been carried out by a hydrothermal microwave-assisted method [55,56]. In particular, a 0.1 mol L^{-1} fresh aqueous solution of Sn (IV) was prepared by adding 3.506 g of $SnCl_4 \cdot 5H_2O$ to 100 ml (pH = 2). Subsequently, 50 ml of that solution were poured in a glass vial and transferred to a monomode microwave oven (Sairem Miniflox 200SS). The solution was then heated at 80 °C for 1 h under magnetic stirring (a maximum of 20 W was applied to maintain that temperature). The suspension was afterwards cooled to room

temperature in few minutes. The obtained white powder was washed by centrifugation (three times with water and once with ethanol) for 20 min. Finally, a part of the powder was dried during 15 h at room temperature under vacuum to carry out the physicochemical characterization analyses. The remaining part of the powder was dispersed in isopropanol (1.33 g_{SnO_2} L^{-1}) to be used as the electrocatalyst in CO_2 electroreduction experiments.

2.2. Gas diffusion electrodes manufacturing

The preparation of SnO_2-GDEs was carried out according to the following procedure: Initially, a carbon-based ink is prepared by mixing carbon powder (Vulcan XC-72R, Cabot, carbon black), and polytetrafluoroethylene (PTFE) (Sigma-Aldrich, 60 wt% dispersion in H_2O) in a mass ratio 40/60. The mixture was then diluted to 3% in isopropanol. The resulting dispersion was airbrushed onto a carbonaceous support (TGP-H-60 with 40% (w/w) PTFE, Toray Inc.) in order to obtain a partially hydrophobic carbon microporous layer (MPL), which was sintered at 623 K for 30 min. Then, a catalytic ink containing the synthesized SnO_2 NPs dispersed in isopropanol and a Nafion solution (5 wt%, Alfa Aesar, copolymer polytetrafluoroethylene) with a (SnO_2+Nafion)/isopropanol mass ratio of 1.6/98.4 was finally airbrushed onto the MPL surface. The geometric surface area (A) of the catalytic layer was 10 cm^2 and the SnO_2 catalytic loading was 0.75 mg cm^{-2}, which were selected according to previous research studies using Sn-GDEs [57]. The final SnO_2 loading was controlled by continuous weighing of the electrode during the airbrushing process. Figure 1 shows a scheme of the as-prepared SnO_2-GDEs configuration.

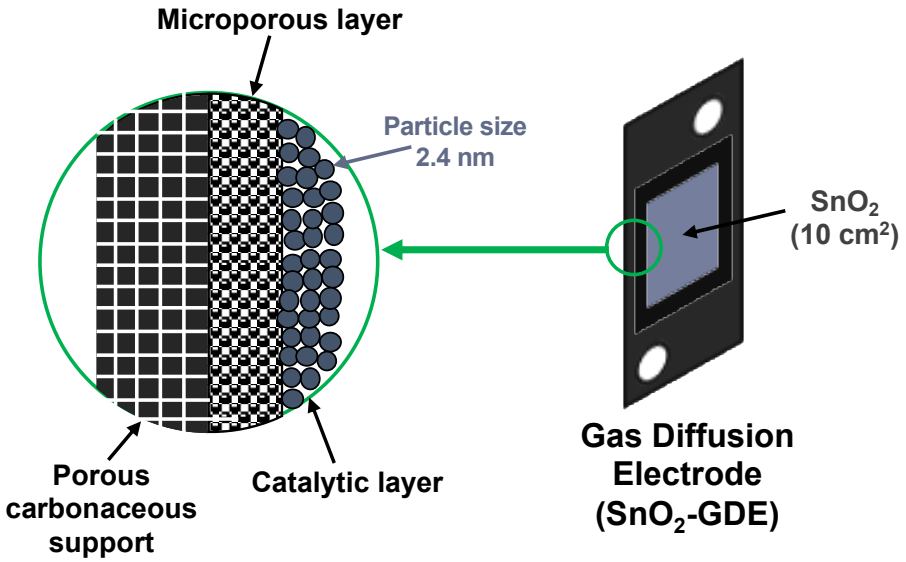

Fig. 1. Graphical representation of the SnO_2-GDE configuration.

2.3. Physicochemical and electrochemical characterization techniques.

The crystalline structure of the SnO_2 NPs was analyzed by powder X-ray diffraction (XRD) on a Bruker D8 Advance X-ray diffractometer in the 20-80° 2θ range using a Cu Kα X-ray irradiation

source (λ= 0.1542 nm). Step time and step size were 1 s and 0.03°, respectively. The specific surface area analysis of the SnO_2 NPs was carried out by N_2 sorption at 77 K using a Belsorb Max (Belsorb Japan). Prior to measurements, SnO_2 NPs were degassed for 15 h under a primary vacuum at 150 °C. The BET method was applied to determine the specific surface area of the electrocatalyst.

The morphology and the average size of the SnO_2 NPs were analyzed by transmission electron microscopy (TEM) using a Tecnai spirit G2 apparatus equipped with a Gatan CCD which operates at 120 kV (LaB6). The samples were prepared by evaporating diluted suspensions in ethanol onto carbon-coated copper grids. It is important to point out that more than 100 particles have been considered on several TEM pictures in order to evaluate the average size of the as-prepared SnO_2 NPs. Furthermore, the conductivity of the SnO_2 NPs was evaluated using impedance spectroscopy. In brief, the conductivity was measured on ~14% SnO_2 NPs pellet (thickness = 1.21 mm and diameter = 13 mm) at room temperature in air, with a frequency range varying between 0.1 and 10^5 Hz and an amplitude of 200 mV_{rms}. The spectra were then analyzed using Zview software for the determination of the electrical conductivity of the SnO_2 NPs.

Cyclic voltammetry (CV) analyses were performed using a CH Instruments 760E potentiostat in a three-electrode configuration electrochemical cell. A glassy carbon (GC) electrode (3 mm in diameter), at which different amounts of the prepared suspension (SnO_2 NPs in isopropanol) were deposited, acted as the working electrode, whereas a graphite rod and an Ag/AgCl (saturated in KCl) were used as the counter and the reference electrodes, respectively. Either CO_2- or Ar-saturated 0.1 M $KHCO_3$ aqueous solutions were used as the electrolyte. The GC electrode was mechanically polished with alumina, sonicated and rinsed with ultrapure water to ensure the complete removal of SnO_2 NPs from previous experiments. The applied potential ranged from 1 V to -1.75 V vs. Ag/AgCl at a scan rate of 100 mV s^{-1}. Potentials reported here were converted to reversible hydrogen electrode (RHE) using the equation: $E_{RHE} = E_{Ag/AgCl} + 0.197 + 0.059pH$.

2.4. CO_2 flow electrolyzer setup and experimental conditions

The manufactured SnO_2-GDEs were tested for CO_2RR in an electrochemical filter-press reactor configuration (Micro Flow Cell, Electrocell A/S), which operated at constant current in continuous mode controlled by a MSTAT4 system (Arbin Instruments). The electrochemical filter-press reactor was divided in two compartments (cathode and anode) by a cationic exchange membrane Nafion® 117. The filter-press configuration can be found elsewhere [58]. Figure 2 shows the CO_2RR continuous reactor scheme using a CO_2 single-pass flow configuration. (0.5 M KCl + 0.45 M $KHCO_3$) and 1 M KOH aqueous solutions were used as catholyte and anolyte, respectively. The effect on CO_2RR selectivity and performance of two experimental parameters was evaluated: the electrolyte flow per geometric electrode area (F/A) (0.57, 0.15 and 0.07 mL min^{-1} cm^{-2}) and the applied current density (from 200 to 500 mA cm^{-2}). It is worth noting here that both the catholyte and the anolyte passed only once throughout the cell (single-pass configuration). The

cathode side was also fed with a pure CO_2 gas stream at a flow of 200 mL min^{-1}. A Dimensionally Stable Anode [DSA/O_2 (Ir-MMO (mixed metal oxide) on Pt)] and a leak-free Ag/AgCl 3.4 mol L^{-1} KCl electrodes were used as the anode and the reference, respectively. Reactor temperature was monitored along the experiment.

Liquid samples were analyzed by ion chromatography aiming at determining the formate concentration. A Dionex ICS 1100 equipped with and AS9-HC column was used as ion chromatograph, with a 4.5 mM Na_2CO_3 aqueous solution as the eluent (at a flow rate of 1 mL min^{-1}) and operated at approximately 13.8 MPa. Some liquid samples were selected to analyze the formation of alcohols by using a headspace gas chromatograph (GCMS-QP2010 Ultra Shimadzu) equipped with a flame ionization detector (FID). Additionally, a four-channel gas microchromatograph (490 Micro GC, Agilent Technologies) equipped with micro thermal conductivity detectors (Micro-TCD) was used for the detection and quantification of gaseous reduction products.

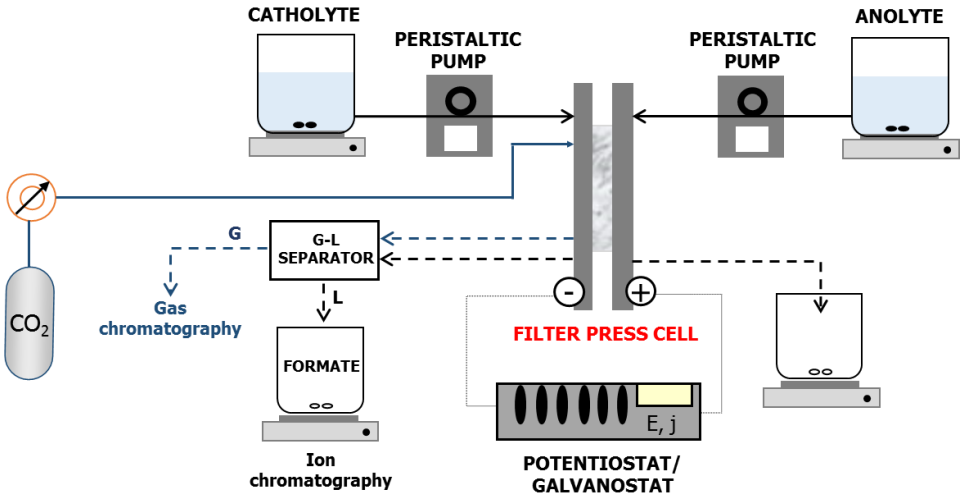

Fig. 2. CO_2RR continuous reactor setup scheme.

The manufactured SnO_2-GDEs were tested for continuous CO_2RR in a single-pass flow reactor at ambient conditions during 90 min electrolyses, where a pseudo-stable performance in time was observed (see Figure S1), as was previously described for Sn-GDEs [58]. Both liquid and gas samples were analyzed by duplicate every 30 min of electrolysis and an averaged concentration of each product (independent of electrolysis time) was calculated and reported herein. Some long-run electrolyses (5 h) were also performed to evaluate the stability of the developed electrocatalyst. Additionally, some figures of merit [59] to describe the CO_2RR were calculated, namely:

The Faradaic efficiency (FE), which represents the percentage of the total charge applied to the system that is actually used to produce any target reduction product (*i.e.* formate), according to the following equation:

$$FE\ (\%) = \frac{z\,n\,F}{Q}\ x\ 100 \qquad (1),$$

where *z* represents the number of electrons exchanged to form the desired product (e.g. *z* = 2 for the electroconversion of CO_2 into formate), *n* corresponds to the number of moles produced, F is the Faraday constant (F = 96,485 C mol^{-1}) and *Q* represents the total charge (C) circulated through the system, which is obtained by multiplying the current applied in amperes and the electrolysis time in seconds.

The production rate (r), which is defined as the productivity (moles) per unit of cathode area (geometric or electroactive area) and time (mmol m^{-2} s^{-1}). r is essential to evaluate the technical feasibility of the process;

$$\text{Geometric rate} = r_G = F/A_G \bullet C_{formate} \quad (2),$$

$$\text{Real rate} = r_R = F/A_R \bullet C_{formate} \quad (3),$$

where (F/A) corresponds to the electrolyte flow per geometric (A_G) or real electrode area (A_R) in L m^{-2} s^{-1} and $C_{formate}$ the concentration of product detected in mmol L^{-1}.

The energy consumption (EC), which represents the required amount of energy used to produce the target product (formate), according to:

$$Energy\ Consumption\ \left(\frac{kWh}{kmol}\right) = \frac{Q \cdot V}{n}\ x\ 2.78 \cdot 10^{-4} \quad (4),$$

where V represents the absolute cell potential in volts.

3. Results and Discussion

3.1. Physicochemical characterization of SnO_2 nanoparticles

The crystalline structure of the synthesized SnO_2 powder is firstly characterized using the X-ray diffraction technique. The obtained pattern presented in Figure 3 is indexed with the tetragonal phase of SnO_2 cassiterite (JCPDS 00-041-1445). Besides, very broad diffraction lines indicate a very small crystallite size, below 5 nm.

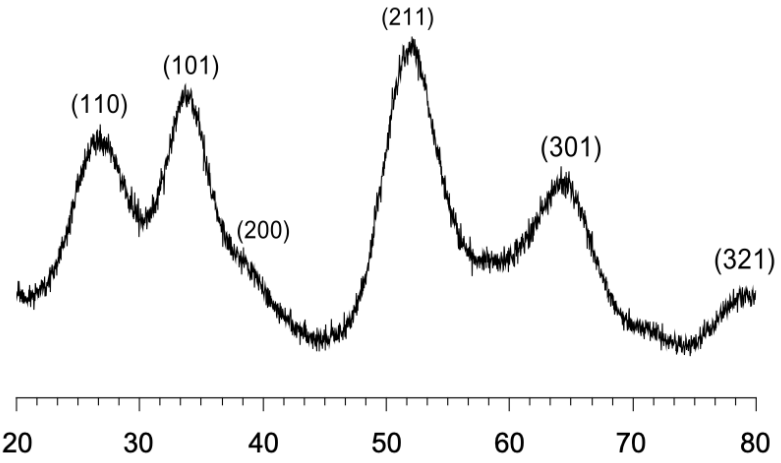

Fig. 3. X-ray diffraction pattern of the synthesized SnO_2 nanoparticles (the diffraction lines are indexed according to the cassiterite structure, JCPDS 00-041-1445).

This fact is further confirmed on the transmission electron micrographs of the synthesized SnO_2 NPs (Figure 4), where a mean size of (2.4 ± 0.6) nm can be measured. SnO_2 NPs are almost spherical and rather monodisperse in size. The surface area of the dried powder was also determined using the BET model and a specific surface area of 299 m^2 g^{-1} was determined for the synthesized SnO_2 NPs, which is significantly larger than the value of commercially available equivalent nanomaterials.

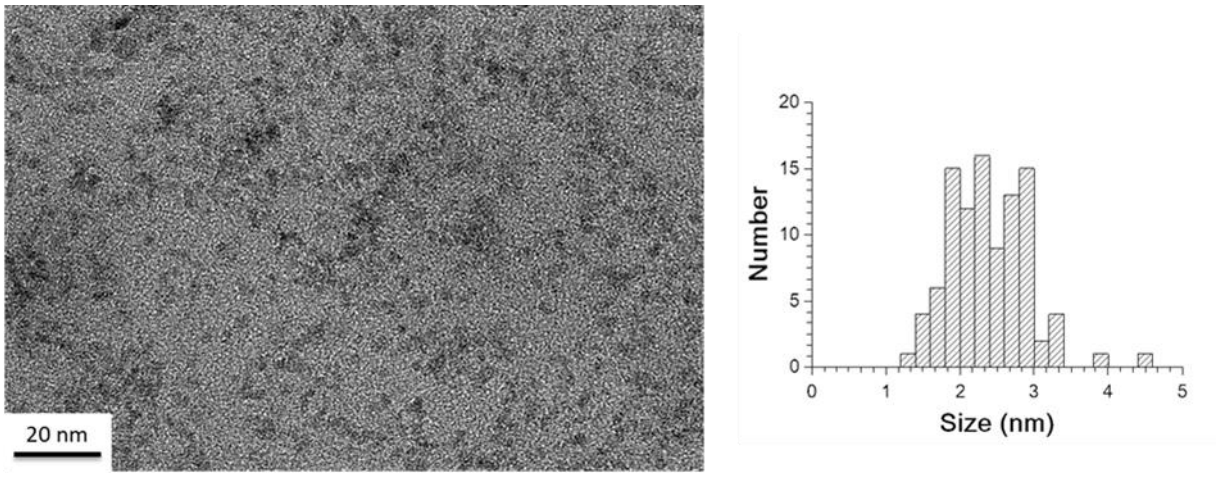

Fig. 4. TEM image of synthesized SnO_2 nanoparticles including its size distribution.

3.2. Electrochemical characterization of SnO_2 nanoparticles

Different voltammeric analyses were carried out to study the electrochemical behavior of SnO_2 NPs in presence and absence of CO_2. In fact, some controversy is present in the literature nowadays regarding the mechanism of CO_2RR on SnO_2, since some reports pointed out SnO_2 and SnO as catalytically active sites for CO_2RR [39,42,45], but others suggested an initial electrochemical reduction step to form metallic Sn^0, which was considered the actual catalytic site [60]. For this reason, we studied small aliquots of SnO_2/isopropanol suspension deposited onto a GC electrode in presence and absence of CO_2. Figure 5a shows a clear and highly symmetrical reduction peak centered at -0.53 V vs RHE in a CO_2 free solution, which decreases rapidly in intensity with consecutive scans. This symmetrical peak shape denotes that the reduction process has taken place on the electrode surface and it is not linked to any electroactive species coming from the solution, which fits the reduction process from SnO_2 to metallic Sn^0 previously reported by Zhang et al. [46]. Moreover, the backward scans show no reversibility in the reduction process observed, since a negligible oxidation current is collected in the anodic sweep. In addition to this, the effect of the amount of SnO_2 NPs deposited onto the electrode surface was also studied, as shown in Figure 5b. The electrochemical response from the deposition of three different amounts of SnO_2 NPs (i.e. 0.133 mg, 0.067 mg and 0.033 mg) was evaluated and lower peak currents

were displayed as the amount of SnO_2 deposited decreases ($8.5\ 10^{-5}$ A, $3.49\ 10^{-5}$ A and $2.20\ 10^{-5}$ A, respectively), which proves that the reduction current observed is proportional to the amount of SnO_2 NPs on the electrode. In contrast, Figure 6 shows a totally different electrochemical behavior displayed by SnO_2 NPs when CO_2 is present in solution. The reduction peak observed in figures 5a and 5b is inhibited and only the hysteresis observed in the cyclic voltammogram in the presence of CO_2 (blue plot in Figure 6) denotes an electrode surface modification, which is subsequently confirmed by the presence of a symmetrical oxidation peak centered at -0.065 V in the anodic scan. This oxidation peak could be attributed to the reoxidation of some metallic Sn^0 previously formed during the cathodic scan in agreement with Lee et al. [39] who has already demonstrated by XRD and XPS the stability of large sized SnO_2 NPs during CO_2RR with only a small fraction of metallic Sn^0 formed at pH 8.4.

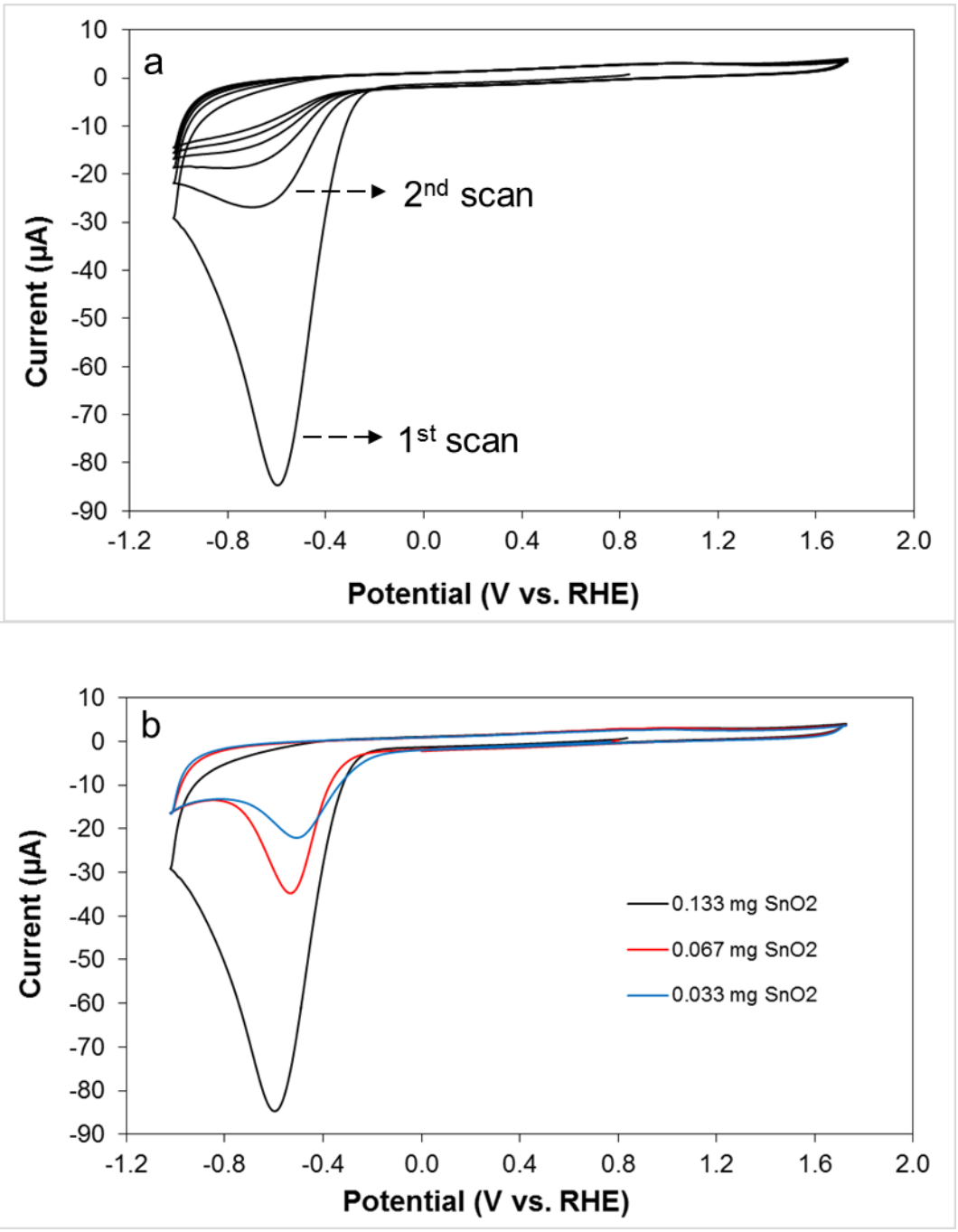

Fig. 5. Cyclic voltammetry of SnO_2 NPs deposited onto a GC electrode in an Ar saturated 0.1 M $KHCO_3$ aqueous solution: a) 0.133 mg SnO_2 NPs are deposited and several consecutive cycles are plotted, and b) effect of SnO_2 loading. Scan rate 100 mV s^{-1}.

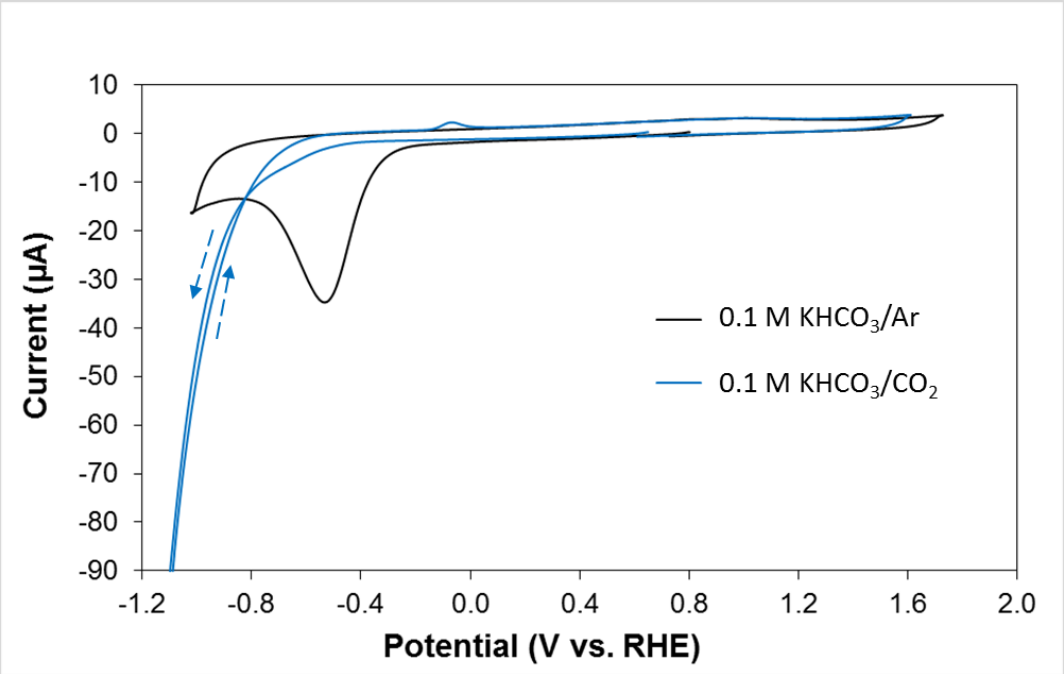

Fig. 6. Cyclic voltammetry of 0.067 mg SnO_2 NPs deposited onto a GC electrode in: (Black plot) an Ar saturated 0.1 M $KHCO_3$ aqueous solution and (Blue plot) a CO_2 saturated 0.1 M $KHCO_3$ aqueous solution. Scan rate 100 mV s^{-1}.

3.3. Continuous CO_2 electroreduction into formate

Two parameters were mainly evaluated on the performance of manufactured SnO_2-GDEs for CO_2RR in a flow electrolyzer: the catholyte flow per geometric electrode area (F/A) (0.57, 0.15 and 0.07 mL min^{-1} cm^{-2}) and the applied current density (from 200 to 500 mA cm^{-2}), since those two parameters were previously identified as key parameters in the production of formate from CO_2RR [22,58,61]. Figure 7 shows that the production of formate, which is a key figure of merit to evaluate the CO_2RR performance, is strongly dependent on both parameters: F/A and current density. Figure 7 exhibits much higher formate concentrations for lower catholyte flows per electrode area in all 3 current densities studied. This trend is in agreement with previously reported results obtained using Sn-GDEs (10-15 nm Sn NPs) for CO_2RR in a very similar flow electrolyzer at current densities between 90 and 200 mA cm^{-2} [58]. Nevertheless, the comparison of formate concentration produced by equivalent experiments performed at 200 mA cm^{-2} in SnO_2-GDEs (1.8 and 12.9 g $HCOO^-$ L^{-1} at 0.57 and 0.07 mL min^{-1} cm^{-2}, respectively) and Sn-GDEs (2.6 and 16.9 g $HCOO^-$ L^{-1} at 0.57 and 0.07 mL min^{-1} cm^{-2}, respectively [58]) highlights a poorer formate productivity in SnO_2-GDEs, in spite of the fact that SnO_2 NPs are significantly smaller in size than Sn NPs used in catalyzing the GDEs and SnO_x have been identified as responsible of enhancing formate production. Thus, the electrical conductivity of the synthesized SnO_2 NPs was evaluated by impedance spectroscopy (10^{-7} S cm^{-1}). This conductivity value is typical in semiconducting materials such as SnO_2, but provokes a significant electrical resistance in the electrode, which become more relevant at high current densities. This fact was experimentally observed by heat

generation in the reactor, which proved energy dissipation. This effect of the ohmic drop on electrode performance has been already addressed in flow electrolyzers for fuel cells [62]. Thus, an estimation of the impact in formate production by the electrical losses converted in heat by Joule effect during CO_2RR (i.e. part of the charge supplied is used in generating heat instead of the reduction of CO_2 to the product of interest) was carried out and suggested that the difference in performance observed between SnO_2-GDEs and Sn-GDEs could be attributed to the moderate conductivity of SnO_2 NPs. Some additional calculations are described in the supplementary information.

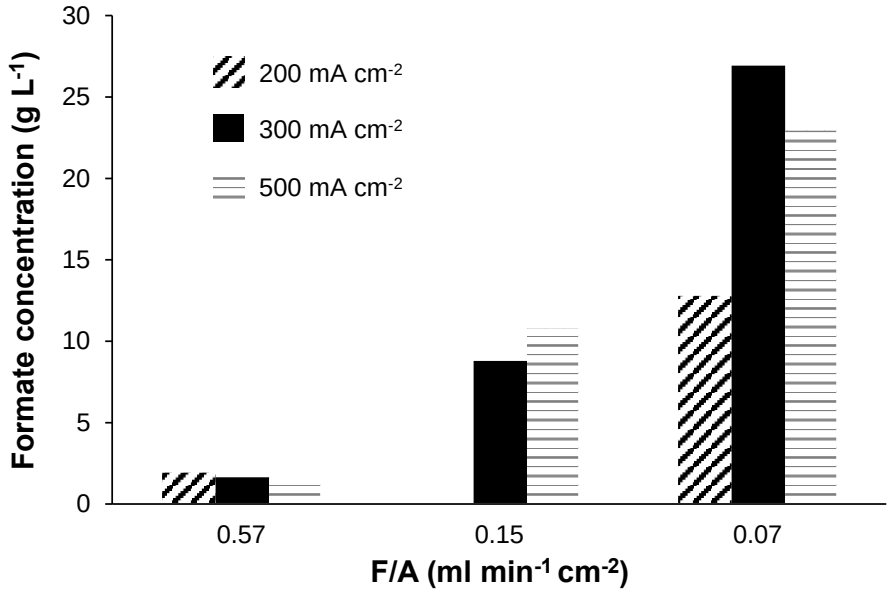

Fig. 7. Formate concentration produced on SnO_2-GDEs at different applied current densities and catholyte flows.

Table 1 presents the quantification of the main products in both liquid and gas-phases and the corresponding figures of merit obtained for CO_2RR performed on the manufactured SnO_2-GDEs in a flow electrolyzer at constant current. The most relevant result displayed in Table 1 corresponds to a formate production of 27 g L^{-1} (entry 5). This is the highest formate concentration value reported on Sn based electrocatalysts using a flow electrolyzer and a catholyte solution in equivalent conditions. Only catholyte-free electrolyzers have been able to produce significantly higher formate concentrations [61,63]. Table 2 compares the best results obtained in the present study and those previously reported in the literature achieved for Sn-GDE and Sn-catalyst coated membrane electrode (CCME) configurations in flow electrolyzers.

Table 1. Formate production rates, concentration, Faradaic efficiencies and energy consumption results at SnO_2-GDEs (metal loading = 0.75 mg cm^{-2}) as a function of the current density and the catholyte flow.

Entry	Geometric current density, j_G (mA cm^{-2})	F/A (mL min^{-1} cm^{-2})	Geometric rate, r_G (mmol m^{-2} s^{-1})	Real rate, r_R (mmol m^{-2} s^{-1})	Formate concentration (g L^{-1})	Formate FE (%)	Energy consumption (kWh $kmol^{-1}$)	Gas-phase FE (%)			
								H_2	CO	C_2H_4	C_3H_8
1	200	0.57	3.87	1.73 10^{-3}	1.8	37.3	933	10.6	0.3	---	1.6
2		0.07	3.33	1.48 10^{-3}	12.9	32.1	1251	27.0	0.3	---	0.3
3	300	0.57	3.52	1.57 10^{-3}	1.7	22.6	2013	10.4	0.2	---	1.3
4		0.15	4.94	2.20 10^{-3}	8.8	31.7	1359	7.0	0.2	---	0.2
5		0.07	6.98	3.11 10^{-3}	27.0	44.9	752	7.6	0.23	---	0.77
6	500	0.57	3.00	1.34 10^{-3}	1.4	11.6	4392	15.3	0.08	0.72	0.8
7		0.15	6.01	2.68 10^{-3}	10.8	23.2	2194	15.7	0.07	0.65	0.57
8		0.07	5.95	2.65 10^{-3}	22.9	23.0	2266	12.1	0.09	0.52	0.8

Table 2. Comparison of our highest CO_2-into-formate result on SnO_2-GDE and some examples from the literature on Sn-GDE and Sn-CCME, in all cases using flow electrolyzers.

Catalyst	Reactor configuration	Pressure (bar)	Temperature (K)	Geometric current density, j_G (mA cm^{-2})	Formate concentration (g L^{-1})	Formate FE (%)
SnO_2-GDE (this work)	Divided single-pass	1	293	300	27	44.9
Sn-GDE [58]	Divided single-pass	1	293	200	16.9	42.3
Sn-CCME [22]	Divided single-pass	1	293	45	19.2	49.4
Sn sheet [64]	Undivided Recirculation	30	293	80	19.2	
Sn-CCME [63]	Divided single-pass	1	343	55.4	41.5	93.3
Sn-CCME [63]	Divided single-pass	1	323	38.5	116.2	77.7

The catholyte flow per geometric electrode area (F/A) and the applied current density were the two parameters evaluated on the results reported in Table 1. Looking first at the effect of current density, two different behaviors can be observed. On the one hand, at high catholyte flow (5.7 mL min^{-1}) formate concentration remained unaffected by the applied current density, 1.8, 1.7 and 1.4 g L^{-1} were detected at 200, 300 and 500 mA cm^{-2}, respectively (entries 1, 3 and 6 in Table 1). This fact provoked a relevant decrease in FE with increasing current density. On the other hand,

at low catholyte flow (0.7 mL min^{-1}) formate concentration, rate and FE described a maximum at 300 mA cm^{-2} together with a minimum in EC of 752 kWh $kmol^{-1}$ (entry 5 in Table 1). Additionally, the increase of applied current density at constant catholyte flow provoked a significant diminution in the total FE of all quantified products, being 59.7% (entry 2) the maximum value achieved among all results reported in Table 1. Looking at the effect of F/A ratio in the results of Table 1, the formate concentration was significantly enhanced by reducing F/A from 0.57 to 0.07 mL min^{-1} cm^{-2} in all 3 current densities. Nevertheless, two different behaviors can be observed. On the one hand, at 200 mA cm^{-2} (entries 1 and 2 in Table 1) formate concentration increased almost linearly (from 1.8 to 12.9 g L^{-1}) by decreasing F/A ratio (from 0.57 to 0.07 mL min^{-1} cm^{-2}) keeping FEs almost constant. On the other hand, at 300 (entries 3, 4 and 5 in Table 1) and 500 mA cm^{-2} (entries 6, 7 and 8 in Table 1) the increase observed in formate concentration (from 1.7 to 27 g L^{-1} and from 1.4 to 22.9 g L^{-1}, respectively) is twice the decrease in percentage of F/A ratio (from 0.57 to 0.07 mL min^{-1} cm^{-2}). This fact together with the diminution in the total FE of all quantified products when higher current densities were applied and formate concentration independent of applied current density at high catholyte flow clearly demonstrated the existence of a leakage of formate by crossover from the catholyte towards the anolyte through the membrane, which was enhanced by increasing the catholyte flow. This phenomenon of formate anions migration towards the anode is negligible working with a cationic exchange membrane like the one used in this work (Nafion 117) at low and moderate current densities (below 200 mA cm^{-2}), but becomes relevant when high current densities are applied. Actually, a large drop in FE due to formate crossover through the Nafion 117 membrane was already described when reducing CO_2 on a metallic Sn^0 electrode in a single pass flow reactor at high applied current [38].

The stability and durability of the SnO_2 NPs catalyzing the CO_2RR on SnO_2-GDEs represent an important issue that needs to be addressed for evaluating the technical and economic feasibility of the CO_2 electroconversion process. Therefore, Figure 8 shows the evolution of formate concentration with electrolysis time under optimal conditions selected from Table 1 (300 mA cm^{-2} and 0.07 mL min^{-1} cm^{-2}). Figure 8 exhibits an almost constant production of formate with time, which demonstrated the long-term stability of SnO_2 NPs during CO_2 electroreduction. It is worth recalling the significant formate concentration achieved after 5 h of electrolysis (27 g L^{-1} = 0.6 M) in comparison with metallic Sn^0 based catalysts from the literature (see Table 2), denoting the possibility of using size-controlled SnO_2 NPs with high specific surface area for an enhanced CO_2 electroconversion into formate. Moreover, this formate concentration is higher than the required one for the use of formate as a fuel in DFAFC for the generation of electricity, which has been reported to be, at least, 0.5 M [65]. Therefore, the use of high surface area SnO_2 NPs in flow electrolyzers may open a novel promising perspective to develop more robust systems for CO_2 electroconversion into formate combined with DFAFCs for energy production.

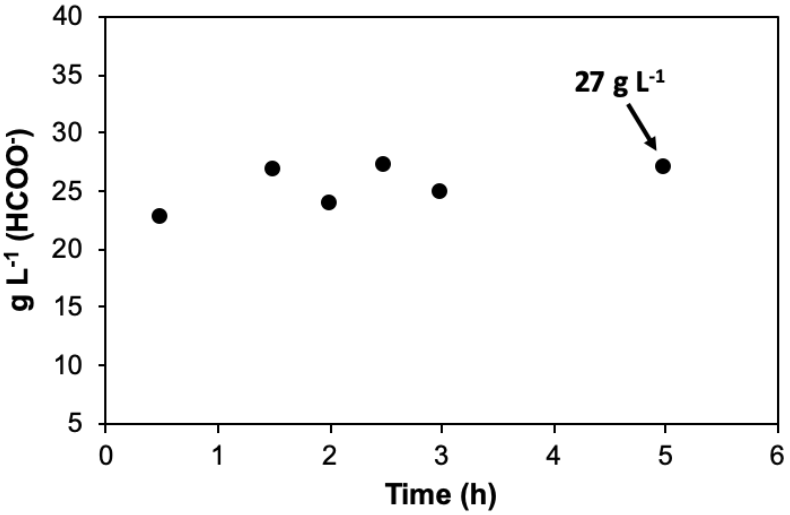

Fig. 8. Continuous formate production as a function of CO_2 electrolysis time on SnO_2-GDE at 300 mA cm^{-2} and F/A = 0.07 mL min^{-1} cm^{-2}

4. Conclusions

Crystalline and high specific surface area SnO_2 NPs (2.4 nm and 299 m^2 g^{-1} in average diameter size and surface area, respectively), synthesized by a facile hydrothermal microwave-assisted method, have been evaluated as an alternative electrocatalyst for the continuous production of formate from CO_2 single-pass electrochemical conversion, at high current density within a flow electrolyzer. So far, activity and selectivity performance of SnO_2 NPs were only reported in a two compartments H-type cell displaying poor current densities.

The electrochemical characterization by cyclic voltammetry of SnO_2 NPs has demonstrated, for the first time (only XRD and XPS proved that before [39, 45]), the high structural stability of SnO_2 under CO_2 reduction conditions, since the reduction peak associated with SnO_2 reduction to metallic Sn^0 present in argon saturated solution is inhibited in the presence of CO_2.

The effect of catholyte flow per geometric electrode area (F/A) (0.57, 0.15 and 0.07 mL min^{-1} cm^{-2}) and applied current density (200, 300 and 500 mA cm^{-2}) were evaluated on the performance of manufactured SnO_2-GDEs for continuous CO_2RR in a single-pass flow reactor at ambient conditions. At a constant current density of 300 mA cm^{-2} and low catholyte flow per electrode area (0.07 mL min^{-1} cm^{-2}), a maximum formate concentration of 27 g L^{-1} was achieved with a FE of 44.9%, a formate production rate of 6.98 mmol m^{-2} s^{-1} and an energy consumption of 752 kWh $kmol^{-1}$. This is the highest formate concentration value reported so far on Sn based electrocatalysts using a flow electrolyzer and a catholyte solution in equivalent conditions. This formate concentration result was only overcome by catholyte free flow electrolyzers, which benefits from a minimal amount of water vapor present as catholyte to carry out the CO_2RR. The FE towards formate using SnO_2 NPs was in the same range as those values reported for Sn-

based electrodes (40-50%), even though higher energy consumption per kmol of formate produced was required at SnO_2-GDEs, which highlights the limited conductivity of SnO_2 NPs.

Poorer formate productivity in SnO_2-GDEs than in Sn-GDEs was observed at 200 mA cm^{-2}, in spite of the fact that SnO_2 NPs were significantly smaller in size than Sn NPs and SnO_x have been identified as responsible of enhancing formate production. This fact pointed out a non-negligible ohmic drop contribution on the SnO_2-GDEs due to the semiconducting properties of SnO_2, which provoked heat generation in the reactor by energy dissipation. However, the electrical losses by Joule effect associated with the ohmic drop during CO_2RR were not large enough to justify the low total FEs obtained (60 - 29 %), even though both liquid and gas-phase products were analyzed. This fact together with the too high increase observed in formate concentration linked to the decrease in F/A ratio at high current densities, as well as formate production independent of applied current density observed at high catholyte flow, demonstrated the existence of a leakage of formate by crossover migration from the catholyte towards the anolyte through the membrane, which was enhanced by increasing the catholyte flow.

In conclusion, this study represents a step forward in the development of strategies based on SnO_2 nanomaterials for the continuous electrochemical conversion of CO_2 into formate since a formate concentration of 27 g L^{-1} (0.6 M), which is superior to the limit for the use of formate as a fuel in DFAFCs, has been achieved during 5 h of operation at 300 mA cm^{-2}. Finally, these results suggest that interesting future research may involve developing SnO_2-based electrodes displaying higher electrical conductivity in order to reduce electrical losses and new ionic membrane separators able to reduce the formate crossover from the catholyte to the anolyte where formate can be oxidized back to CO_2. This will allow to significantly increase the efficiency of formate production from CO_2RR on SnO_2 NPs at high current densities.

Acknowledgements

The authors gratefully acknowledge the financial sources from the Spanish Ministry of Economy and Competitiveness (MINECO), through the project CTQ2016-76231-C2-1-R (AEI/FEDER, UE). Moreover, I.M.-G. and C.M. S.-S would like to thank the MINECO for the postdoctoral period in Paris of the predoctoral research contract (BES-2014-070081) and J. A. for the Ramón y Cajal programme (RYC-2015-17080), respectively. L.T. and O.D. acknowledge the support of French governmental funds managed by the ANR within the Investissements d'Avenir programme under reference ANR-11-IDEX-0004-02, and more specifically within the framework of the Cluster of Excellence MATISSE led by Sorbonne Université.

References

[1] National Oceanic & Atmospheric Administration (NOAA), Trends in Atmospheric Carbon Dioxide, Mauna Loa Observatory (MLO, Hawaii), Earth Syst. Res. Lab. (2020)

https://www.esrl.noaa.gov/gmd/ccgg/trends/monthly.

[2] X. Lu, D.Y.C. Leung, H. Wang, M.K.H. Leung, J. Xuan, Electrochemical Reduction of Carbon Dioxide to Formic Acid, ChemElectroChem. 1 (2014) 836–849. https://doi.org/10.1002/celc.201300206.

[3] J.T. Song, H. Song, B. Kim, J. Oh, Towards higher rate electrochemical CO2 conversion: From liquid-phase to gas-phase systems, Catalysts. 9 (2019) 224. https://doi.org/10.3390/catal9030224.

[4] T. Sakakura, J.C. Choi, H. Yasuda, Transformation of carbon dioxide, Chem. Rev. 107 (2007) 2365–2387. https://doi.org/10.1021/cr068357u.

[5] I. Merino-Garcia, E. Alvarez-Guerra, J. Albo, A. Irabien, Electrochemical membrane reactors for the utilisation of carbon dioxide, Chem. Eng. J. 305 (2016) 104–120. https://doi.org/10.1016/j.cej.2016.05.032.

[6] J. Albo, M. Alvarez-Guerra, A. Irabien, Electro-, photo- and-photoelectro-chemical reduction of CO2, in: Heterog. Catal. Emerg. Tech. Des. Charact. Appl., Wiley-VCH, 2020.

[7] J.L. White, M.F. Baruch, J.E. Pander, Y. Hu, I.C. Fortmeyer, J.E. Park, T. Zhang, K. Liao, J. Gu, Y. Yan, T.W. Shaw, E. Abelev, A.B. Bocarsly, Light-Driven Heterogeneous Reduction of Carbon Dioxide: Photocatalysts and Photoelectrodes, Chem. Rev. 115 (2015) 12888–12935. https://doi.org/10.1021/acs.chemrev.5b00370.

[8] A. Taheri, L.A. Berben, Making C-H bonds with CO2: production of formate by molecular electrocatalysts, Chem. Commun. 52 (2016) 1768–1777. https://doi.org/10.1039/c5cc09041e.

[9] C. Costentin, M. Robert, J.M. Savéant, Catalysis of the electrochemical reduction of carbon dioxide, Chem. Soc. Rev. 42 (2013) 2423–2436. https://doi.org/10.1039/c2cs35360a.

[10] E.E. Benson, C.P. Kubiak, A.J. Sathrum, J.M. Smieja, Electrocatalytic and homogeneous approaches to conversion of CO2 to liquid fuels, Chem. Soc. Rev. 38 (2009) 89–99. https://doi.org/10.1039/b804323j.

[11] E. Vichou, Y. Li, M. Gomez-Mingot, M. Fontecave, C.M. Sánchez-Sánchez, Imidazolium-And Pyrrolidinium-Based Ionic Liquids as Cocatalysts for CO2 Electroreduction in Model Molecular Electrocatalysis, J. Phys. Chem. C. 124 (2020) 23764–23772. https://doi.org/10.1021/acs.jpcc.0c07556.

[12] S. Nitopi, E. Bertheussen, S.B. Scott, X. Liu, A.K. Engstfeld, S. Horch, B. Seger, I.E.L. Stephens, K. Chan, C. Hahn, J.K. Nørskov, T.F. Jaramillo, I. Chorkendorff, Progress and Perspectives of Electrochemical CO2 Reduction on Copper in Aqueous Electrolyte,

Chem. Rev. 119 (2019) 7610–7672. https://doi.org/10.1021/acs.chemrev.8b00705.

[13] C.M. Sánchez-Sánchez, J. Souza-Garcia, E. Herrero, A. Aldaz, Electrocatalytic reduction of carbon dioxide on platinum single crystal electrodes modified with adsorbed adatoms, J. Electroanal. Chem. 668 (2012) 51–59. https://doi.org/10.1016/j.jelechem.2011.11.002.

[14] L. Zhang, I. Merino-Garcia, J. Albo, C.M. Sánchez-Sánchez, Electrochemical CO2 reduction reaction on cost-effective oxide-derived copper and transition metal–nitrogen–carbon catalysts, Curr. Opin. Electrochem. 23 (2020) 65–73. https://doi.org/10.1016/j.coelec.2020.04.005.

[15] H.K. Ju, G. Kaur, A.P. Kulkarni, S. Giddey, Challenges and trends in developing technology for electrochemically reducing CO2 in solid polymer electrolyte membrane reactors, J. CO2 Util. 32 (2019) 178–186. https://doi.org/10.1016/j.jcou.2019.04.003.

[16] R. Kortlever, J. Shen, K.J.P. Schouten, F. Calle-Vallejo, M.T.M. Koper, Catalysts and Reaction Pathways for the Electrochemical Reduction of Carbon Dioxide, J. Phys. Chem. Lett. 6 (2015) 4073–4082. https://doi.org/10.1021/acs.jpclett.5b01559.

[17] C.M. Sánchez-Sánchez, V. Montiel, D.A. Tryk, A. Aldaz, A. Fujishima, Electrochemical approaches to alleviation of the problem of carbon dioxide accumulation, Pure Appl. Chem. 73 (2001) 1917–1927. https://doi.org/10.1351/pac200173121917.

[18] J. Wu, Y. Huang, W. Ye, Y. Li, CO2 Reduction: From the Electrochemical to Photochemical Approach, Adv. Sci. 4 (2017) 1700194. https://doi.org/10.1002/advs.201700194.

[19] J. Qiao, Y. Liu, F. Hong, J. Zhang, A review of catalysts for the electroreduction of carbon dioxide to produce low-carbon fuels, Chem. Soc. Rev. 43 (2014) 631–675. https://doi.org/10.1039/c3cs60323g.

[20] C. Delacourt, P.L. Ridgway, J.B. Kerr, J. Newman, Design of an Electrochemical Cell Making Syngas (CO +H2) from CO2 and H2O Reduction at Room Temperature, J. Electrochem. Soc. 155 (2007) B42–B49. https://doi.org/10.1149/1.2801871.

[21] I. Merino-Garcia, J. Albo, P. Krzywda, G. Mul, A. Irabien, Bimetallic Cu-based hollow fibre electrodes for CO2 electroreduction, Catal. Today. 346 (2020) 34–39. https://doi.org/10.1016/j.cattod.2019.03.025.

[22] G. Díaz-Sainz, M. Alvarez-Guerra, J. Solla-Gullón, L. García-Cruz, V. Montiel, A. Irabien, Catalyst coated membrane electrodes for the gas phase CO2 electroreduction to formate, Catal. Today. 346 (2020) 58–64. https://doi.org/10.1016/j.cattod.2018.11.073.

[23] J. García, C. Jiménez, F. Martínez, R. Camarillo, J. Rincón, Electrochemical reduction of CO2 using Pb catalysts synthesized in supercritical medium, J. Catal. 367 (2018) 72–80.

https://doi.org/10.1016/j.jcat.2018.08.017.

[24] J. Albo, A. Sáez, J. Solla-Gullón, V. Montiel, A. Irabien, Production of methanol from CO2 electroreduction at Cu2O and Cu2O/ZnO-based electrodes in aqueous solution, Appl. Catal. B Environ. 176–177 (2015) 709–717. https://doi.org/10.1016/j.apcatb.2015.04.055.

[25] D. Ren, Y. Deng, A.D. Handoko, C.S. Chen, S. Malkhandi, B.S. Yeo, Selective Electrochemical Reduction of Carbon Dioxide to Ethylene and Ethanol on Copper(I) oxide catalysts, ACS Catal. 5 (2015) 2814–2821. https://doi.org/10.1021/cs502128q.

[26] I. Merino-Garcia, J. Albo, A. Irabien, Productivity and Selectivity of Gas-Phase CO2 Electroreduction to Methane at Copper Nanoparticle-Based Electrodes, Energy Technol. 5 (2017) 922–928. https://doi.org/10.1002/ente.201600616.

[27] I. Merino-Garcia, J. Albo, J. Solla-Gullón, V. Montiel, A. Irabien, Cu oxide/ZnO-based surfaces for a selective ethylene production from gas-phase CO2 electroconversion, J. CO2 Util. 31 (2019) 135–142. https://doi.org/10.1016/j.jcou.2019.03.002.

[28] Z. Cai, Y. Wu, Z. Wu, L. Yin, Z. Weng, Y. Zhong, W. Xu, X. Sun, H. Wang, Unlocking bifunctional electrocatalytic activity for CO2 reduction reaction by win-win metal-oxide cooperation, ACS Energy Lett. 3 (2018) 2816–2822. https://doi.org/10.1021/acsenergylett.8b01767.

[29] X. Yu, P.G. Pickup, Recent advances in direct formic acid fuel cells (DFAFC), J. Power Sources. 182 (2008) 124–132. https://doi.org/10.1016/j.jpowsour.2008.03.075.

[30] S. Ponnurangam, I. V. Chernyshova, P. Somasundaran, Nitrogen-containing polymers as a platform for CO2 electroreduction, Adv. Colloid Interface Sci. 244 (2017) 184–198. https://doi.org/10.1016/j.cis.2016.09.002.

[31] C. Oloman, H. Li, Electrochemical processing of carbon dioxide, ChemSusChem. 1 (2008) 385–391. https://doi.org/10.1002/cssc.200800015.

[32] U.O. Nwabara, E.R. Cofell, S. Verma, E. Negro, P.J.A. Kenis, Durable Cathodes and Electrolyzers for the Efficient Aqueous Electrochemical Reduction of CO2, ChemSusChem. 13 (2020) 855–875. https://doi.org/10.1002/cssc.201902933.

[33] A. Irabien, M. Alvarez-Guerra, J. Albo, A. Dominguez-Ramos, Electrochemical conversion of CO2 to value-added products, in: Electrochem. Water Wastewater Treat., Elsevier, Amsterdam, 2018: pp. 29–59.

[34] N. Han, P. Ding, L. He, Y. Li, Y. Li, Promises of Main Group Metal–Based Nanostructured Materials for Electrochemical CO2 Reduction to Formate, Adv. Energy Mater. 10 (2020) 1902338. https://doi.org/10.1002/aenm.202070046.

[35] G. Díaz-Sainz, M. Alvarez-Guerra, J. Solla-Gullón, L. García-Cruz, V. Montiel, A. Irabien,

CO2 electroreduction to formate: Continuous single-pass operation in a filter-press reactor at high current densities using Bi gas diffusion electrodes, J. CO2 Util. 34 (2019) 12–19. https://doi.org/10.1016/j.jcou.2019.05.035.

[36] D. Wu, G. Huo, W.Y. Chen, X.Z. Fu, J.L. Luo, Boosting formate production at high current density from CO2 electroreduction on defect-rich hierarchical mesoporous Bi/Bi2O3 junction nanosheets, Appl. Catal. B Environ. 271 (2020) 118957. https://doi.org/10.1016/j.apcatb.2020.118957.

[37] D. Pavesi, R.C.J. Van De Poll, J.L. Krasovic, M. Figueiredo, G.J.M. Gruter, M.T.M. Koper, K.J.P. Schouten, Cathodic Disintegration as an Easily Scalable Method for the Production of Sn-and Pb-Based Catalysts for CO2Reduction, ACS Sustain. Chem. Eng. 8 (2020) 15603–15610. https://doi.org/10.1021/acssuschemeng.0c04875.

[38] H. Li, C. Oloman, Development of a continuous reactor for the electro-reduction of carbon dioxide to formate - Part 2: Scale-up, J. Appl. Electrochem. 37 (2007) 1107–1117. https://doi.org/10.1007/s10800-007-9371-8.

[39] S. Lee, J.D. Ocon, Y. Il Son, J. Lee, Alkaline CO2 electrolysis toward selective and continuous HCOO- production over SnO2 nanocatalysts, J. Phys. Chem. C. 119 (2015) 4884–4890. https://doi.org/10.1021/jp512436w.

[40] B. Kumar, V. Atla, J.P. Brian, S. Kumari, T.Q. Nguyen, M. Sunkara, J.M. Spurgeon, Reduced SnO2 Porous Nanowires with a High Density of Grain Boundaries as Catalysts for Efficient Electrochemical CO2-into-HCOOH Conversion, Angew. Chemie - Int. Ed. 56 (2017) 3645–3649. https://doi.org/10.1002/anie.201612194.

[41] Y. Chen, M.W. Kanan, Tin oxide dependence of the CO2 reduction efficiency on tin electrodes and enhanced activity for tin/tin oxide thin-film catalysts, J. Am. Chem. Soc. 134 (2012) 1986–1989. https://doi.org/10.1021/ja2108799.

[42] Yiliguma, Z. Wang, C. Yang, A. Guan, L. Shang, A.M. Al-Enizi, L. Zhang, G. Zheng, Sub-5 nm SnO2 chemically coupled hollow carbon spheres for efficient electrocatalytic CO2 reduction, J. Mater. Chem. A. 6 (2018) 20121–20127. https://doi.org/10.1039/c8ta08058e.

[43] C. Zhao, J. Wang, J.B. Goodenough, Comparison of electrocatalytic reduction of CO2 to HCOOH with different tin oxides on carbon nanotubes, Electrochem. Commun. 65 (2016) 9–13. https://doi.org/10.1016/j.elecom.2016.01.019.

[44] R. Zhang, W. Lv, L. Lei, Role of the oxide layer on Sn electrode in electrochemical reduction of CO2 to formate, Appl. Surf. Sci. 356 (2015) 24–29. https://doi.org/10.1016/j.apsusc.2015.08.006.

[45] Y. Fu, Y. Li, X. Zhang, Y. Liu, J. Qiao, J. Zhang, D.P. Wilkinson, Novel hierarchical SnO2 microsphere catalyst coated on gas diffusion electrode for enhancing energy efficiency

of CO2 reduction to formate fuel, Appl. Energy. 175 (2016) 536–544. https://doi.org/10.1016/j.apenergy.2016.03.115.

[46] S. Zhang, P. Kang, T.J. Meyer, Nanostructured tin catalysts for selective electrochemical reduction of carbon dioxide to formate, J. Am. Chem. Soc. 136 (2014) 1734–1737. https://doi.org/10.1021/ja4113885.

[47] J. Wu, F.G. Risalvato, S. Ma, X.D. Zhou, Electrochemical reduction of carbon dioxide III. The role of oxide layer thickness on the performance of Sn electrode in a full electrochemical cell, J. Mater. Chem. A. 2 (2014) 1647–1651. https://doi.org/10.1039/c3ta13544f.

[48] A. Kuzume, A. Dutta, S. Vesztergom, P. Broekmann, Operando raman spectroscopy: Studies on the Reactivity and Stability of SnO2 Nanoparticles During Electrochemical CO2 Reduction Reaction, in: Encycl. Interfacial Chem. Surf. Sci. Electrochem., Elsevier, 2018: pp. 217–226. https://doi.org/10.1016/B978-0-12-409547-2.13300-1.

[49] F.D. Mayer, P. Hosseini-Benhangi, C.M. Sánchez-Sánchez, E. Asselin, E.L. Gyenge, Scanning electrochemical microscopy screening of CO2 electroreduction activities and product selectivities of catalyst arrays, Commun. Chem. 3 (2020) 155. https://doi.org/10.1038/s42004-020-00399-6.

[50] G. Liu, Z. Li, J. Shi, K. Sun, Y. Ji, Z. Wang, Y. Qiu, Y. Liu, Z. Wang, P.A. Hu, Black reduced porous SnO2 nanosheets for CO2 electroreduction with high formate selectivity and low overpotential, Appl. Catal. B Environ. 260 (2020) 118134. https://doi.org/10.1016/j.apcatb.2019.118134.

[51] F. Li, L. Chen, G.P. Knowles, D.R. MacFarlane, J. Zhang, Hierarchical Mesoporous SnO2 Nanosheets on Carbon Cloth: A Robust and Flexible Electrocatalyst for CO2 Reduction with High Efficiency and Selectivity, Angew. Chemie. 56 (2017) 505–509. https://doi.org/10.1002/ange.201608279.

[52] E. Jeng, F. Jiao, Investigation of CO2 single-pass conversion in a flow electrolyzer, React. Chem. Eng. 5 (2020) 1768–1775. https://doi.org/10.1039/d0re00261e.

[53] S. Malkhandi, B.S. Yeo, Electrochemical conversion of carbon dioxide to high value chemicals using gas-diffusion electrodes, Curr. Opin. Chem. Eng. 26 (2019) 112–121. https://doi.org/10.1016/j.coche.2019.09.008.

[54] P. Jeanty, C. Scherer, E. Magori, K. Wiesner-Fleischer, O. Hinrichsen, M. Fleischer, Upscaling and continuous operation of electrochemical CO2 to CO conversion in aqueous solutions on silver gas diffusion electrodes, J. CO2 Util. 24 (2018) 454–462. https://doi.org/10.1016/j.jcou.2018.01.011.

[55] B.L. Caetano, F. Meneau, C. V. Santilli, S.H. Pulcinelli, M. Magnani, V. Briois, Mechanisms of SnO2 nanoparticles formation and growth in acid ethanol solution

derived from SAXS and combined raman-XAS time-resolved studies, Chem. Mater. 26 (2014) 6777–6785. https://doi.org/10.1021/cm5032688.

[56] M. Krishna, S. Komarneni, Conventional- vs microwave-hydrothermal synthesis of tin oxide, SnO2 nanoparticles, Ceram. Int. 35 (2009) 3375–3379. https://doi.org/10.1016/j.ceramint.2009.06.010.

[57] A. Del Castillo, M. Alvarez-Guerra, J. Solla-Gullón, A. Sáez, V. Montiel, A. Irabien, Electrocatalytic reduction of CO2 to formate using particulate Sn electrodes: Effect of metal loading and particle size, Appl. Energy. 157 (2015) 165–173. https://doi.org/10.1016/j.apenergy.2015.08.012.

[58] A. Del Castillo, M. Alvarez-Guerra, J. Solla-Gullón, A. Sáez, V. Montiel, A. Irabien, Sn nanoparticles on gas diffusion electrodes: Synthesis, characterization and use for continuous CO2 electroreduction to formate, J. CO2 Util. 18 (2017) 222–228. https://doi.org/10.1016/j.jcou.2017.01.021.

[59] C.M. Sánchez-Sánchez, E. Expósito, J. Solla-Gullón, V. García-García, V. Montiel, A. Aldaz, Calculation of the characteristic performance indicators in an electrochemical process, J. Chem. Educ. 80 (2003) 529. https://doi.org/10.1021/ed080p529.

[60] J. Gu, F. Héroguel, J. Luterbacher, X. Hu, Densely Packed, Ultra Small SnO Nanoparticles for Enhanced Activity and Selectivity in Electrochemical CO2 Reduction, Angew. Chemie - Int. Ed. 57 (2018) 2943–2947. https://doi.org/10.1002/anie.201713003.

[61] G. Díaz-Sainz, M. Alvarez-Guerra, A. Irabien, Continuous electrochemical reduction of CO2 to formate: Comparative study of the influence of the electrode configuration with Sn and Bi-based electrocatalysts, Molecules. 25 (2020) 4457. https://doi.org/10.3390/molecules25194457.

[62] Y. Bultel, P. Ozil, R. Durand, Modelling the mode of operation of PEMFC electrodes at the particle level: Influence of ohmic drop within the active layer on electrode performance, J. Appl. Electrochem. 28 (1998) 269–276. https://doi.org/10.1023/A:1003207514936.

[63] W. Lee, Y.E. Kim, M.H. Youn, S.K. Jeong, K.T. Park, Catholyte-Free Electrocatalytic CO2 Reduction to Formate, Angew. Chemie - Int. Ed. 57 (2018) 6883–6887. https://doi.org/10.1002/anie.201803501.

[64] F. Proietto, B. Schiavo, A. Galia, O. Scialdone, Electrochemical conversion of CO2 to HCOOH at tin cathode in a pressurized undivided filter-press cell, Electrochim. Acta. 277 (2018) 30–40. https://doi.org/10.1016/j.electacta.2018.04.159.

[65] L. An, R. Chen, Direct formate fuel cells: A review, J. Power Sources. 320 (2016) 127–139. https://doi.org/10.1016/j.jpowsour.2016.04.082.